Influence of Nonlinear Irregular Waves on the Fatigue Loads of an Offshore Wind Turbine

Michiel B. van der Meulen[1], Turaj Ashuri[2], Gerard J.W. van Bussel[3] and David P. Molenaar[1]

[1] Offshore Center of Competence, Siemens, the Netherlands
[2] Department of Aerospace Engineering, University of Michigan, Ann Arbor, USA
[3] Faculty of Aerospace Engineering, Delft University of Technology, the Netherlands

E-mail: michiel_van.der.meulen@siemens.com

Abstract. In order to make offshore wind power a cost effective solution that can compete with the traditional fossil energy sources, cost reductions on the expensive offshore support structures are required. One way to achieve this, is to reduce the uncertainty in wave load calculations by using a more advanced model for wave kinematics. As offshore wind turbines are generally sited in shallow water, nonlinear effects which results in steeper waves with higher velocities and accelerations are common. Whereas extreme waves are modeled with higher-order nonlinear regular wave models, fatigue loads are calculated from kinematics obtained by a low-fidelity linear irregular wave model. In this paper, a second-order wave model that is employed to simulate the dynamic response due to nonlinear irregular waves on a full set of IEC-standard load cases. This method is computationally efficient, which is particularly useful for design optimization studies. It is shown that by using this method for a 25 m deep site in the German Bight, equivalent fatigue loads increase by 7.5 % compared to the traditional linear wave model. The effect of nonlinear waves on fatigue is most prevalent in the foundation and tower parts near the sea surface. Furthermore, it is found that the increase in fatigue damage accumulation is most prevalent in wind-wave misaligned load cases, in which aerodynamic damping is absent.

1. Introduction

Going offshore and upscaling are the current technological trends in wind energy. Upscaling poses several fundamental design challenges mainly on the rotor [1], and going offshore makes in general the design more expensive than onshore wind turbines [2]. Cost reduction of the support structures has a fundamental importance, since it acts as a bottleneck to the realization of offshore wind farms that can compete with traditional energy sources [3].

Currently, offshore wind farms are typically sited in coastal areas with water depths around or less than 30 m [4, 5]. For these water depths, the monopile foundation type is by far the most popular. Due to the limited water depth, nonlinear effects cause the waves to become more sharp-crested while the troughs are flattened. Besides that, the magnitude of particle velocities and accelerations below the waves are higher, which leads to higher hydrodynamic loads on the wind turbine support structure.

In the kinematic wave models used in offshore engineering, irregular waves are usually approximated with classical linear (Airy) wave theory [6]. Since this method only describes wave kinematics up to the mean sea level, Wheeler stretching [7] is often applied to redistribute the

velocity and acceleration profiles up to the actual sea surface, but other extension and stretching methods exist and are sometimes used instead [8]. This traditional approach, based on deep water experience from the oil and gas industry is accurate enough when the wave amplitude is small with respect to water depth, but in shallow water kinematics magnitudes are likely to be underestimated.

In order to be able to account for strong nonlinear effects in the highest waves that may occur during the lifetime of an offshore structure, a nonlinear regular wave model such as the analytical 5^{th}-order Stokes method or a numerical Fourier approximation based on stream function theory is commonly employed [9, 10]. This separate deterministic extreme wave is inserted in a stochastic wave record, such that in a aero-servo-elastic simulation of an extreme wave in the time-domain, the turbine dynamics due to an irregular sea state are included in the simulation.

Whereas in extreme wave events nonlinear effects are thus accounted for, a nonlinear model for irregular waves is uncommon in engineering practice. To compensate for the lack of accuracy of linear wave theory in shallow water, a safety factor is usually applied to obviate an underestimation of wave loads. Using a more accurate irregular wave model, the amount of uncertainty in fatigue load estimation could be lowered, which may lay the ground for a discussion on the safety factor that is used. Altough nonlinear irregular waves are expected to result in higher wave loads, the possible safety factor reduction might still result in a lower structural mass and hence reduced cost.

When it comes to modeling nonlinear irregular waves, there are several options. The second-order nonlinear irregular wave model developed by Sharma and Dean [11] is the one that has received the most attention in similar research topics. In this model, which is a second-order perturbation expansion of linear wave theory, the contribution of sum- and difference frequencies are added to the first-order solution from linear wave theory. The Hybrid wave model by Zhang [12] is a similar model with the addition of nonlinear effects due to short waves riding on top of larger waves, which are empirically mixed with the results of second-order theory. Fully nonlinear waves can be modeled with more advanced Boussinesq models [13], but since these are very computationally expensive, using this type of model is outside the scope of this research. Since the second-order wave model is mentioned as an alternative for linear wave theory in DNV Recommended Practice (DNV-RP-C205) [14], this is the model that will be used for this research.

To this date, knowledge about the influence of nonlinear irregular waves on offshore wind turbine fatigue loads is fairly limited. Several studies provided evidence that fatigue loads due to nonlinear irregular waves will increase [15, 16, 17]. A recent load extrapolation study by Agarwal [18] showed that long-term loads increase with approximately 10% when using nonlinear waves. It must be remarked that this study was limited to two governing environmental states only, in which the significant wave height was high with respect to the water depth.

In general however, a large part of the wind turbine fatigue life is consumed during operation in mild conditions, in which nonlinear effects are much weaker. Therefore it may very well be the case that the overall fatigue load increase is less than the mentioned 10%. However, such an investigation of the influence of nonlinear waves on fatigue while taking into account a full set of design load cases (IEC Standards 61400-3) [19], is not known by the author. This paper therefore aims at analyzing the influence of nonlinear irregular waves on response behavior and fatigue load for a complete set of load cases with a realistic design configuration, rather than inspecting a single environmental state or using a simplified structural model. Additionally, since the method employs a frequency domain formulation, it is computationally very efficient. This trick together with some other useful techniques developed by the authors [20, 21] enables design optimization studies where several thousand of function evaluations per optimization iteration are required.

This paper is structured as follows: First, the methods required to generate time-series of

hydrodynamic loads on offshore wind turbines are presented. This comprises the procedure to generate a random wave record, the theoretical formulation of linear and second-order wave theory and the Morison equation to predict hydrodynamic loads from wave kinematics time-series. We then present the results of the second-order wave model simulations. The qualitative effect of the second-order contributions on a typical wave record and the spectral representation of the sea surface elevation and in-line bending moment are shown. The result of using nonlinear wave loads as input in the dynamic response simulation, which is carried out by the Siemens software package BHawC in the time-domain, is then presented. In these simulations, a Siemens wind turbine from a wind farm in the German Bight, supported by a monopile foundation, is used. Next, we present the results of the calculated equivalent fatigue load and make a comparison with the outcome of simulations performed with the wave loads from the linear wave model. Finally, the paper is concluded by an analysis of the observations, conclusions and recommendations for follow-up research.

2. Methodology

In order to simulate the dynamic response due to the hydrodynamic forces acting on a monopile support structure, time-series of the hydrodynamic load for a number of vertical coordinates has to be realized. Regardless of the type of model that is used for wave kinematics, the empirical Morison equation is currently considered to be the most appropriate tool to create these time-series. In the Morison equation, the drag and inertia forces due to horizontal fluid particle velocities and accelerations, U and $\dot{U}$ respectively, are added together to estimate the total in-line wave force:

$$f_{Morison} = f_D + f_I = \frac{1}{2}\rho C_d D\,|U|\,U + \rho C_m \frac{\pi D^2}{4}\dot{U} \tag{1}$$

where ρ and D denote the water density and structural diameter, respectively. The magnitude of the force components furthermore strongly depends on a proper selection of appropriate values for the added inertia and drag force coefficients, C_m and C_d. In this formulation, structural motion is ignored, but the Morison equation can easily be extended to use the relative wave kinematics instead, see for example [18]. To account for diffraction effects, the MacCamy-Fuchs correction can be applied as a low-pass filter on the acceleration terms [22]. Since this is a correction to account for linear diffraction only, in this paper the MacCamy-Fuchs correction is assumed to be valid on first-order acceleration terms only.

In many occasions, a current due to tidal motion is to be taken into account. Since the interaction between currents and wave kinematics is hard to predict and thus to model, a simple assumption is often made to simply vectorially add a steady current velocity profile to the wave kinematics. Additionally, the Doppler shift that appears in the observed wave frequency observed from a stationary frame of reference, can be taken into account [23].

2.1. Simulation of linear and nonlinear irregular waves

The common approach to simulate a random wave field is to take a high number of frequency components, and use linear superposition to create an irregular wave record. This superposition of random waves and the application of linear wave theory to predict wave kinematics is described in many textbooks, for example [24, 25]. According to linear wave theory, the first-order surface elevation can be expressed as follows:

$$\eta^{(1)}(t) = \sum_{m=1}^{N} a_m \cos(\omega_m t - k_m x - \phi_m) \tag{2}$$

Randomness in the simulations is obtained by uniformly distributing the phase angles ϕ_m between 0 and 2π. Besides that, the amplitudes a_m follow from the Rayleigh distributed

amplitude variances, which has an expected value that is obtained from the wave spectrum: $E(a_m^2) = 2S(\omega_m)\Delta\omega$. The wave number k_m is related to the angular frequency ω_m through the linear dispersion relation, $\omega_m^2 = gk_m \tanh(k_m d)$, where d is the water depth below mean sea level.

To ensure randomness, a high number of frequencies, typically more than 200, is desirable [25]. The maximum or cut-off frequency of the simulations, if not bounded by the Nyquist sampling criterion, can be assumed four times the peak frequency of the wave spectrum [26]. Using this cut-off frequency, a good compromise between frequency discretization density and simulation bandwidth is achieved.

According to classical linear wave theory, the 1$^{\text{st}}$-order velocity potential that corresponds to the surface elevation given in Eq. 2 reads:

$$\Phi^{(1)}(z,t) = \sum_{m=1}^{N} b_m \frac{\cosh k_m(z+d)}{\cosh k_m d} \sin(\omega_m t - k_m x - \phi_m) \tag{3}$$

where b_m are the amplitude coefficients given by:

$$b_m = \frac{a_m g}{\omega_m} \tag{4}$$

In the reference system used in these expressions, x is positive in the propagation direction of the waves. For a monopile support structure, x can simply be assumed zero. The vertical coordinate z is positive upward and is zero at mean sea level. By deriving the velocity potential, expressions for the first-order horizontal velocity and acceleration can be obtained :

$$U^{(1)}(z,t) = \frac{\partial \Phi^{(1)}}{\partial x}\,, \quad \dot{U}^{(1)}(z,t) = \frac{\partial}{\partial t}\left(\frac{\partial \Phi^{(1)}}{\partial x}\right) \tag{5}$$

For the second-order nonlinear irregular wave model by Sharma and Dean [11], similar expressions can be derived for the sea surface elevation and kinematics. The second-order accurate sea surface elevation, being a perturbation expansion of the first-order formulation, reads:

$$\eta^{(2)}(t) = \eta^{(1)} + \Delta\eta^{(2)} \tag{6}$$

Here, $\Delta\eta^{(2)} = \Delta\eta^{(2+)} + \Delta\eta^{(2-)}$ is the second-order perturbation, which comprises the difference- and sum frequency corrections given by:

$$\Delta\eta^{(2)}(t) = \sum_{m=1}^{N}\sum_{n=1}^{N}\left[a_m a_n \left\{B_{mn}^{-}\cos(\psi_m - \psi_n) + B_{mn}^{+}\cos(\psi_m + \psi_n)\right\}\right] \tag{7}$$

The expressions for the transfer functions of the 2$^{\text{nd}}$-order amplitude, B_{mn}^{-} and B_{mn}^{+}, are lengthy and are therefore given in the Appendix section. Furthermore, ψ_m and ψ_n are short notations of the argument in the cosine in Eq. 2:

$$\psi_m = \omega_m t - k_m x - \phi_m \tag{8}$$

The second-order difference- and sum velocity potential that corresponds to the surface elevation perturbations from Eq. 7 read:

$$\Delta\Phi^{(2)}(z,t) = \frac{1}{4}\sum_{m=1}^{N}\sum_{n=1}^{N}\left[b_m b_n \frac{\cosh k_{mn}^{\pm}(z+d)}{\cosh k_{mn}^{\pm} d}\frac{D_{mn}^{\pm}}{(\omega_m \pm \omega_n)}\sin(\psi_m \pm \psi_n)\right] \tag{9}$$

In a similar fashion as for the first-order kinematics, second-order perturbation contributions can be obtained by deriving the above velocity potential.

2.2. Frequency-domain formulation

The linear and second-order nonlinear irregular wave models are formulated in the time-domain. As a large number of waves is to be superimposed, especially the double-summations in the second-order model will be time consuming. To avoid the numerical inefficiency of performing summations in the time-domain, a better approach is to carry out the calculations in the frequency-domain and subsequently use the Inverse Fast Fourier Transform (IFFT) to realize a time series.

This approach based on the Discrete Fourier Transform requires that the frequency components are equally spaced, such that $\omega_m = m\Delta\omega$, where $m = 1, 2, \ldots, N$. For each frequency component m, the Fourier coefficients for the first-order surface elevation, $X^{(1)}_{\eta,m}(\omega)$, are then calculated as follows:

$$X^{(1)}_{\eta,m}(\omega_m) = a_m \exp(-i\phi_m) \tag{10}$$

The IFFT can then be employed to create a time-series from the Fourier coefficients corresponding to the frequency samples ω_m:

$$\eta^{(1)}(t_p) = \Re\left\{\text{IFFT}\left[X^{(1)}_{\eta,m}\right]\right\} \tag{11}$$

where $t_p = p\Delta t$ are the discrete time samples with $p = 1, 2, \ldots, N$. In a similar way, Fourier coefficients for the 1$^{\text{st}}$-order horizontal velocity and acceleration can be calculated and a time-series can be realized for each z-coordinate. Since the number of required summations is not astronomical, the time gain by using a frequency-domain approach for the linear wave model is limited. This is quite different for the second-order expressions, as will be shown below. The Fourier coefficients of the second-order surface elevation components $\Delta\eta^{(2)}$, as defined by Eq. 7, can calculated by:

$$X^{(2)}_{\eta,mn}(\omega_m, \omega_n) = a_m a_n B^{\pm}_{mn} \exp(-i(\phi_m \pm \phi_n)) \tag{12}$$

Since $m = n = 1, 2, \ldots, N$, the double summation causes the number of Fourier coefficients and therefore the required amount of Fourier transforms to be N^2 rather than N. However, since an equal spacing is used in the frequency discretization, the coefficients with an equal difference or sum frequency can be collected together in a single-summation Fourier coefficient $Y_{\eta,j}$. This collection of the Fourier coefficients for difference and sum contributions, with the indices $j^- = |m - n|$ and $j^+ = m + n$ respectively, is described in great detail by Agarwal [18]. Provided that the number of time samples is adjusted according to the new number of frequency samples in the replacement time vector t_q, the second-order contributions can be transformed to a time-series with the IFFT:

$$\Delta\eta^{(2)}(t_q) = \Re\left\{\text{IFFT}\left[Y^{(2)}_{\eta,j}\right]\right\} \tag{13}$$

This procedure is fully accurate and considerably reduces the amount of required Fourier transforms from N^2 to $2N$, since the highest sum frequency is $(N + N)\Delta\omega$. Similarly, the Fourier coefficients for the second-order kinematics can be calculated and collected in a single-summation form.

3. Comparison of results obtained from different wave models

In this Section, the results from simulations using the second-order wave model are compared with the traditional approach using linear wave theory. First, an overview of the qualitative characteristics of nonlinear waves is presented using results from a simulation of a single sea state. Next, the influence of nonlinear wave modeling on equivalent fatigue load is presented from the time-domain simulations that have been performed on a realistic offshore wind turbine configuration. Here, all design load cases as specified by IEC standards are used in the fatigue load accumulation.

3.1. Qualitative characteristics of second-order wave simulations

To illustrate the behavior of the second-order nonlinear irregular wave model in a qualitative way, Figure 1 shows two snapshots of a surface elevation time series with a comparison between a linear and a nonlinear wave. Two types of waves are shown: the top figure **(a)** represents a regular wave and in the bottom figure **(b)** an irregular wave is depicted. To illustrate how the difference- and sum terms contribute to the 2nd-order wave, these perturbations are shown separately in both graphs.

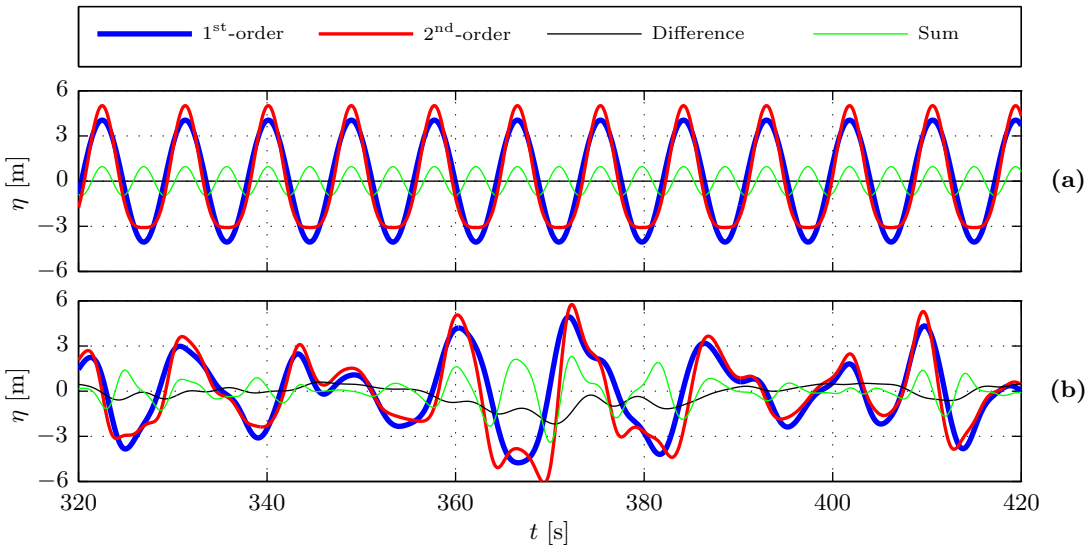

Figure 1. The 1st- and 2nd-order surface elevation for a regular **(a)** and an irregular wave **(b)**. The sum-contributions are responsible for the typical nonlinear sharp crests and flat troughs, while the difference-terms cause a setdown of the water level below a group of large waves. Sea state: $H_S = 8.1$ m, $T_P = 13.1$ s, $\gamma = 3.3$ and water depth $d = 20$ m.

The regular wave shows that the 2nd-order wave features the sharpened crests and flattened troughs that are typical for nonlinear waves. Contrary to the regular wave, where only sum-interactions appear in the wave record, the difference terms do contribute to the 2nd-order wave in the irregular sea surface. It can be observed that the difference interactions produce a long wave that causes a setdown of the water level below high wave groups and a slight water level rise in the calmer parts of the sea surface.

Besides the time-series analysis, we can inspect the behavior in the frequency-domain. In Figure 2 **(a)**, the wave spectrum of the linear and nonlinear sea surface elevation is compared with the JONSWAP spectrum that was used to generate the waves. The results show the average of 500 wave simulations. It can be observed that the linear wave model returns the same spectrum, while the second-order model shows additional low- and high-frequency peaks. The low frequency energy is added by the difference-interactions, while a second addition near 0.15 Hz follows from the sum-interactions, which as expected peaks at approximately twice the peak frequency. Although the 2nd-order model results in a higher spectral power than the theoretical JONSWAP shape, this additional power does not need to be corrected for since typically it also appears in the results from sea surface elevation measurements [17].

An impression of the influence of second-order wave simulations on wave loads can be shown by the Power Spectral Density (PSD) of the in-line bending moment, which is shown in Figure 2 **(b)**. A simple monopile with a diameter of 6 m. and force coefficients $C_D = 1$ and $C_m = 2$ were assumed for this simulation. It can be observed that the sum-frequencies cause a

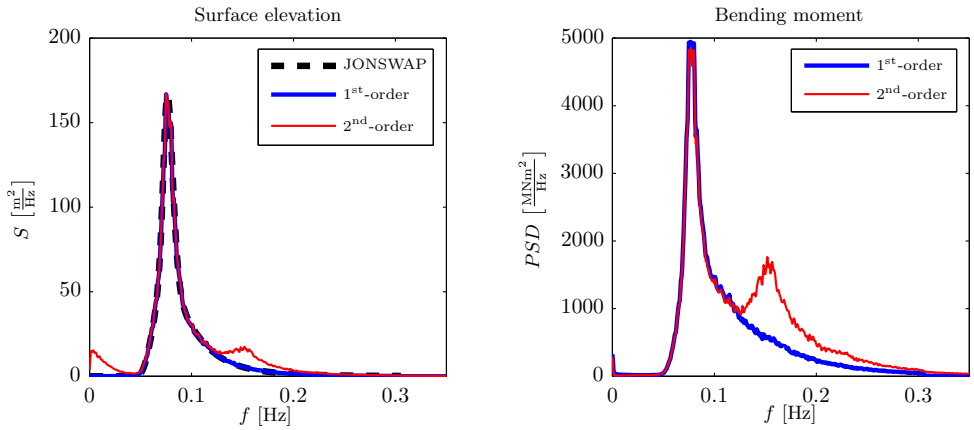

Figure 2. Wave spectrum of the surface elevation**(a)** and PSD of the in-line bending moment **(b)**, averaged over 500 first- and second-order wave model simulations, using a JONSWAP input spectrum. Sea state: $H_S = 8.1$ m, $T_P = 13.1$ s, $\gamma = 3.3$ and water depth $d = 20$ m.

significant increase in bending moment power near twice the peak frequency, while the difference contribution is hardly noticeable.

3.2. Equivalent fatigue loads due to nonlinear wave simulation

The nonlinear irregular wave model presented in this paper is used to produce hydrodynamic load time-series for a Siemens offshore wind turbine, which is supported by a monopile foundation. The soil-structure interaction is also considered based on the work of [27]. The site is located in the German Bight, with a water depth of approximately 25 m. Currents are assumed to be acting in the direction of the waves in all load cases, while the change in observed frequency due to the Doppler shift is ignored. All load cases are taken into account, which means that the difference in equivalent fatigue load between the wave models gives a good indication of the influence of nonlinear waves on fatigue life. Besides that, the wind turbine components that are influenced by nonlinear wave modeling can be identified.

The equivalent fatigue load was evaluated for the bending moments in various components of the offshore wind turbine. Effects on the shaft, hub and blades appeared to be insignificant (¡ 1%) and are therefore not mentioned further in this section. The analysis can thus be constrained to the tower and the foundation supporting the wind turbine. Since the effect on torsion proved to be neglibible, only the influence of nonlinear waves on the bending moment around the axes perpendicular and parallel to the wind direction is assessed. The results of the equivalent fatigue load as a percentage of the linear wave results are shown in Tables 1 and 2.

It can be observed that the foundation is affected most by the higher wave loads, while nonlinear waves only influence the tower in the lower part. Also in the foundation, the highest sensitivity to nonlinear wave action is found near the foundation/tower interface. A significant difference is found in the equivalent fatigue loads between the bending moment axes. The results show that fatigue loads due to bending moments around the axis parallel to wind direction are much higher than those around the axis perpendicular to the wind. This means that an increase in wave loads acting perpendicular to the wind has significantly more influence than higher wave loads in the wind direction.

Furthermore, an analysis on the origin of the increased fatigue loads reveiled that one load case in particular was influencing fatigue loads. This load case DLC 6.4, in which the wind turbine is idling in high wind speeds, only one wave seed was responsible for a relatively high contribution to fatigue damage.

Table 1. Equivalent fatigue load due to the bending moment around the axis perpendicular to the wind direction. Linear waves = 100 %. Wöhler exponent: 3.5 (Tower) and 5.0 (Foundation)

	Linear waves [%]	Nonlinear waves [%]
Tower		
Top	100	100
Interface	100	101.5
Foundation		
Interface	100	102.1
Seabed	100	101.7

Table 2. Equivalent fatigue load due to the bending moment around the axis parallel to the wind direction. Linear waves = 100 %. Wöhler exponent: 3.5 (Tower) and 5.0 (Foundation)

	Linear waves [%]	Nonlinear waves [%]
Tower		
Top	100	100
Interface	100	103.5
Foundation		
Interface	100	107.5
Seabed	100	104.9

4. Analysis and conclusion

It was shown that for a typical monopile supported offshore wind turbine in 25 m. deep water, the equivalent fatigue load on the support structure increases with 7.5 % when nonlinear irregular waves are used in dynamic response simulation. This is obtained by simulating all the load cases required by IEC standards, and it is a confirmation and good match with the results obtained by [17]. It was found that the largest difference in fatigue damage accumulation is caused by waves perpendicular to the wind, which indicates that wind-wave misalignment is important to the increase in fatigue loads due to nonlinear waves. This can be explained by the aerodynamic damping effect of the rotor, which is much less effective at attenuating the response loads when wind and waves are not in line. Furthermore it was noticed that the influence of nonlinear waves is most prevalent near the interface between support structure and tower. A direct conclusion can not be drawn from this observation.

The simulations also reveiled that a single wave seed was responsible for a high amount of fatigue damage in a load case with environmental conditions above the cut-out wind speed. Since the particular wind speed at which this was observed only used one wave seed, randomness of the simulations could cause an unexpected high fatigue damage. This research will therefore be continued with a larger amount of wave seeds.

5. Recommendations for future work

Since nonlinear effects become more pronounced in shallower water, it is expected that nonlinear irregular waves will have a larger influence on fatigue loads when the water depth is further reduced. A similar in-depth analysis for a wind farm situated in shallower water is therefore

strongly recommended for a follow-up research. Besides the influence of depth, evidence exists that fatigue loads may be affected by the shape of the input spectrum that is chosen to generate the random waves [17]. A sensitivity study should be carried out to quantify this influence.

Furthermore, the authors have observed that modeling the action due to a current is often somewhat ambiguous in the industry: out of conservatism currents are sometimes assumed to act only in wave propagation direction, and the effect of a Doppler shift is not always applied. An assessment of the impact of these assumptions on fatigue loads is thus recommended to provide ground for a well-founded decision upon the method to model currents. Finally, it is expected that directional waves will decrease hydrodynamic loads [16]. The current assumption that waves act in a single direction may hence be conservative for fatigue load estimation. One of the challenges in modeling multi-directional waves however, is to obtain the directional wave spectrum, since wave propagation direction is both hard to measure and very site-specific [24].

Appendix - Additional transfer functions in second-order wave model

The transfer functions used in the second-order amplitudes are given as follows:

$$B^{-}_{mn} = \frac{1}{4}\left[\frac{D^{-}_{mn} - (k_m k_n + R_m R_n)}{\sqrt{R_m R_n}} + (R_m + R_n)\right] \tag{14}$$

$$B^{+}_{mn} = \frac{1}{4}\left[\frac{D^{+}_{mn} - (k_m k_n - R_m R_n)}{\sqrt{R_m R_n}} + (R_m + R_n)\right] \tag{15}$$

where

$$\begin{aligned} D^{-}_{mn} =& \frac{\left(\sqrt{R_m} - \sqrt{R_n}\right)\ \left\{\sqrt{R_n}(k_m^2 - R_m^2) - \sqrt{R_m}(k_n^2 - R_n^2)\right\}}{\left(\sqrt{R_m} - \sqrt{R_n}\right)^2 - k^{-}_{mn}\tanh k^{-}_{mn} d} \\ &+ 2\frac{\left(\sqrt{R_m} - \sqrt{R_n}\right)^2 (k_m k_n + R_m R_n)}{\left(\sqrt{R_m} - \sqrt{R_n}\right)^2 - k^{-}_{mn}\tanh k^{-}_{mn} d} \end{aligned} \tag{16}$$

$$\begin{aligned} D^{+}_{mn} =& \frac{\left(\sqrt{R_m} + \sqrt{R_n}\right)\ \left\{\sqrt{R_n}(k_m^2 - R_m^2) + \sqrt{R_m}(k_n^2 - R_n^2)\right\}}{\left(\sqrt{R_m} + \sqrt{R_n}\right)^2 - k^{+}_{mn}\tanh k^{+}_{mn} d} \\ &+ 2\frac{\left(\sqrt{R_m} + \sqrt{R_n}\right)^2 (k_m k_n - R_m R_n)}{\left(\sqrt{R_m} + \sqrt{R_n}\right)^2 - k^{+}_{mn}\tanh k^{+}_{mn} d} \end{aligned} \tag{17}$$

The reduced wave numbers R_m, R_n, and the difference- and sum wave numbers k^{-}_{mn}, k^{+}_{mn} are given by:

$$R_m = \frac{\omega_m^2}{g} \tag{18}$$

$$k^{-}_{mn} = |k_m - k_n| \tag{19}$$

$$k^{+}_{mn} = k_m + k_n \tag{20}$$

References

[1] T. Ashuri and M.B. Zaaijer. Size effect on wind turbine blade's design driver. In *European Wind Energy Conference and Exhibition, Brussels, Belgium*, pages 1–6, 2008. 1

[2] B. Erdogan, Y. Mehmet, and S. Abdulkadir. Offshore wind power development in europe and its comparison with onshore counterpart. *Ren. and Sust. Energy Reviews*, 15(2):905–915, 2011. 1

[3] T. Ashuri. *Beyond Classical Upscaling: Integrated Aeroservoelastic Design and Optimization of Large Offshore Wind Turbines*. PhD thesis, Delft University of Technology, the Netherlands, 2012. 1

[4] S.P. Breton and G. Moe. Status, plans and technologies for offshore wind turbines in europe and north america. *Ren. Energy*, 34(3):646–654, 2009. 1

[5] T. Ashuri and M.B. Zaaijer. Review of design concepts, methods and considerations of offshore wind turbines. In *European Offshore Wind Conference and Exhibition, Berlin, Germany*, pages 1–10, 2007. 1

[6] G.B. Airy. Tides and waves. *Encyclopaedia Metropolitana*, 1845. 1

[7] J.D. Wheeler. Methods for calculating forces produced on piles in irregular waves. *J. of Petr. Tech.*, 1:1–2, 1970. 1

[8] O.T. Gudmestad. Measured and predicted deep water wave kinematics in regular and irregular seas. *Marine Struct.*, 6(1):1–73, 1993. 1

[9] J.D. Fenton. A fifth-order stokes theory for steady waves. *J. of Waterway, Port, Coastal and Ocean Eng.*, 111(2):216–234, 1985. 1

[10] J.D. Fenton. Numerical methods for nonlinear waves. *Adv. in Coastal and Ocean Eng.*, 5:241–324, 1999. 1

[11] J.N. Sharma and R.G. Dean. Second-order directional seas and associated wave forces. *Old SPE J.*, 21(1):129–140, 1981. 1, 2.1

[12] J. Zhang, L. Chen, M. Ye, and R.E. Randall. Hybrid wave model for unidirectional irregular waves, part I. theory and numerical scheme. *Appl. Ocean Res.*, 18(2):77–92, 1996. 1

[13] P.A. Madsen, H.B. Bingham, and H. Liu. A new boussinesq method for fully nonlinear waves from shallow to deep water. *J. of Fluid Mech.*, 462(1):1–30, 2002. 1

[14] Det Norske Veritas. *Recommended practice - DNV-RP-C205 - Environmental conditions and environmental loads*. DNV, 2007. 1

[15] A.R. Henderson and P.W. Cheng. Wave loads on slender offshore structures: Comparison of theory and measurement. In *German Wind Energy Conf. [DEWEK]*, 2002. 1

[16] K. Mittendorf, M. Kohlmeier, A. Habbar, and W. Zielke. Influence of irregular wave kinematics description on fatigue load analysis of offshore wind energy structures. In *Proc. of DEWEK*, pages 22–23, 2006. 1, 5

[17] H.F. Veldkamp and J. Van Der Tempel. Influence of wave modelling on the prediction of fatigue for offshore wind turbines. *Wind Energy*, 8(1):49–65, 2005. 1, 3.1, 4, 5

[18] P. Agarwal and L. Manuel. Incorporating irregular nonlinear waves in coupled simulation and reliability studies of offshore wind turbines. *Appl. Ocean Res.*, 2011. 1, 2, 2.2

[19] International Electrotechnical Commission. *IEC-61400-3 - Wind Turbines: Part 3: Design Requirements for Offshore Wind Turbines*. IEC, 2009. 1

[20] T. Ashuri, M.B. Zaaijer, G.J.W. van Bussel, and G.A.M. van Kuik. An analytical model to extract wind turbine blade structural properties for optimization and up-scaling studies. In *The Science of Making Torque from Wind, Crete, Greece*, pages 1–7, 2010. 1

[21] T. Ashuri, M.B. Zaaijer, G.J.W. van Bussel, and G.A.M. van Kuik. Controller design automation for aeroservoelastic design optimization of wind turbines. In *The Science of Making Torque from Wind, Crete, Greece*, pages 1–7, 2010. 1

[22] R.C. MacCamy and R.A. Fuchs. Wave forces on piles: A diffraction theory. Technical report, DTIC Document, 1954. 2

[23] O.T. Gudmestad and D.T. Karunakaran. Wave current interaction. In *Environmental Forces on Offshore Structures and Their Predictions: Proc. of an Int. Conf.*, 1990. 2

[24] L.H. Holthuijsen. *Waves in oceanic and coastal waters*. Cambridge Univ Pr, 2007. 2.1, 5

[25] S.K. Chakrabarti. *Handbook of offshore engineering*, volume 1. Elsevier, 2005. 2.1, 2.1

[26] G.Z. Forristall. Wave crest distributions: Observations and second-order theory. *J. of Phys. Oceanography*, 30(8):1931–1943, 2000. 2.1

[27] R. Haghi, T. Ashuri, P.L.C. van der Valk, and D.P. Molenaar. Integrated multidisciplinary constrained optimization of offshore support structures. In *The Sciense of Making Torque from Wind, Oldenburg, Germany*, 2012. 3.2